The Numerical Solution of the One-Dimensional Advection–Diffusion Equation in Layered Coordinates

WILLIAM K. DEWAR

Department of Oceanography and Supercomputer Computations Research Institute, The Florida State University, Tallahassee, Florida

TREVOR J. MCDOUGALL

CSIRO Marine Research, Hobart, Tasmania, Australia

(Manuscript received 19 March 1999, in final form 30 September 1999)

ABSTRACT

The numerical solution of the vertical advection–diffusion equation in layered coordinates is revisited. The objectives of this work are to propose a generalization of the discontinuous layered representation of the ocean tracer field to higher-order, smoother representations (while retaining the quasi-Lagrangian character of the coordinate) and compare the solutions generated by several approaches in order to illustrate their respective advantages and disadvantages. The one-dimensional advection–diffusion equation is chosen as a test bed for layered coordinates because ocean simulation for climatic purposes requires the inclusion of dianeutral diffusive processes.

The layered approach is generalized by replacing the traditional stack of well-mixed layers by stacks of piecewise smooth profiles. All the well-known properties of quasi-Lagrangian coordinates are retained. Comparisons of the quasi-Lagrangian solutions with coarse- and fine-resolution fixed grid solutions illustrates the efficiency of the adaptive, quasi-Lagrangian coordinate.

1. Introduction

A potentially powerful way of modeling the ocean involves the so-called quasi-Lagrangian approach, in which the vertical coordinate of the model is a function of the model state. Isopycnic coordinate codes are a well-known example of this model type, and their applications include inverse models (Wunsch 1996 and references therein) and predictive dynamical models (Bleck and Chassignet 1994). Tracers, like potential temperature and salinity, are often viewed in such models as well mixed in the vertical. Thus the vertical structure of the model includes a series of discontinuities of tracer values at layer interfaces.

Advantages of this representation include that it can be made dynamically consistent (i.e., the structure of the velocity field matches that of the tracers) and that exact knowledge of the tracer field in the vertical can be claimed. The last point is equivalent to the idea that the evolution of the system in the vertical dimension can be computed with no errors due to vertical discretization. A disadvantage of this representation is that the real ocean, the replication of which ultimately is the goal of all models, does not consist of a stack of well-mixed tracer layers, but is more aptly described as continuously stratified. Although one may envision that in the limit of many layers the traditional layered approach yields solutions arbitrarily close to those of a continuously stratified fluid, the convergence properties of this approach are not well studied and modern simulations have not yet employed very many layers. Also, conceptual issues may be clouded by the discontinuous representation. In short, the stack of well-mixed layers representation of traditional quasi-Lagrangian modeling constitutes both a strength and a weakness of the approach.

We are thus motivated to consider the above-stated disadvantages. In this paper, we construct a quasi-Lagrangian system that avoids the above weakness of the layered approach by adopting a tracer profile continuous in the vertical. At the same time, we retain the related advantages of the layered approach. With a decision about the desired smoothness of the tracer profiles, perfect knowledge of the tracer fields at all points in the

Corresponding author address: Dr. William K. Dewar, Department of Oceanography (4320), The Florida State University, Tallahassee, FL 32306-4320.
E-mail: dewar@ocean.fsu.edu

vertical can be claimed and the system evolution can be computed without suffering vertical truncation errors. This is analogous to the case in McDougall and Dewar (1998), where a discontinuous representation of the tracers was adopted. In addition, the coordinates are quasi-Lagrangian, can be neutral in character, and can retain the associated desirable properties (e.g., migration to areas, like fronts, where resolution is desired). The physically desirable properties of a diffusive system, with one caveat, can also be guaranteed, for example, downgradient fluxes, perfect conservation of tracers, the ability to work under a variety of boundary conditions, removal of curvature in the S–θ plane, etc. (see McDougall and Dewar 1998). However, extension to smooth tracer profiles does introduce an indirect nonlocal (in the vertical) character to mixing that must be considered physically as a disadvantage. Finally, we illustrate the impacts of these advantages, and the disadvantage, by comparing the solutions so generated with those from coarse- and fine-resolution fixed grid numerical solutions of the one-dimensional advection–diffusion equation (1DADE).

We choose to work with the 1DADE because the advantages usually ascribed to the layered quasi-Lagrangian approach are clearest in the adiabatic oceanic limit. In particular, this approach facilitates the capture of flow invariants. Obvious examples are potential vorticity, potential temperature, and salinity, and it is in this capacity that the layered approach has been found to be very useful in analytical and process numerical modeling (see, e.g., Bleck and Boudra 1981; Pedlosky 1987). A pressing issue of modern importance, however, is the numerical simulation of climate. The emphasis in these studies falls on a number of temporal scales, from seasonal to interannual and beyond. The lower frequencies of the climate system, and quite possibly the higher ones as well, are sensitive to diabatic processes. Since the seminal work by Bryan (1987), connections between the vertical diffusivity of tracers and the strength of the overturning cell have become of central interest to climate theoreticians and modelers.

The above advantage of the layered approach still carries over to the real oceanic case in that the oceans are almost adiabatic in character. The principal transport of tracers occurs along neutral surfaces (McDougall 1987a) and the dianeutral transport is recognized as being orders of magnitude weaker. However, this in principle also makes the accurate modeling of dianeutral dynamics a subtle numerical issue with many well-know pitfalls of significant climatic importance (Veronis 1975). The simplest representation of many of these effects is found within the 1DADE, where diffusion determines the dianeutral velocity.

In classical z coordinate models, perhaps the most widely used models for climate work, the ‘‘Veronis effect’’ (i.e., the spurious dianeutral flux of tracer caused by horizontal tracer transport) has been virtually eliminated due to some recent parameterization advances (Gent and McWilliams 1990; Griffies et al. 1998; Hirst and McDougall 1998). Thus, the dianeutral diffusion within the model is placed much more at the control of the modeler. [Griffies et al. (2000), however, argue numerical errors in the advection operators can effect spurious dianeutral transports]. For linear equations of state, the Veronis effect is by construction entirely absent from layered models. For nonlinear equations of state, however, cabbeling and thermobaricity generate dianeutral fluxes that can be subtle to correctly include in a layered model. Also, the proper way to model dianeutral transport in a layered fluid has not been obvious. In a recent paper, McDougall and Dewar (1998) recommend a dianeutral mixing parameterization for use in layered models that handles many of these issues, thus making isopycnal layered models a viable candidate for climate modeling (see also Hu 1996). Hybrid coordinates represent a different approach to modeling that also addresses the above issues in a layered context; see Schopf and Loughe (1995) for a recent discussion.

The purpose of this paper is to further develop the representation of mixing in layered models by proposing higher-order generalizations of the scheme and comparing the performance of several methods. Our proposed generalization of the quasi-Lagrangian approach to piecewise continuous profiles has an analog in the higher-order finite-difference schemes used in fixed coordinate systems. We also suggest the adaptive nature of the Lagrangian scheme makes this approach efficient with regard to the accurate rendering of tracer profiles in coarsely resolved models.

This paper considers only tracer equations. In this sense, our higher-order techniques are ready to be used in inverse models. Full implementation of these ideas in a numerical primitive equation model must await the consideration of several issues, such as the consistent representation of the velocity field, the inclusion of full equation of state, and connection of the interior with a mixed layer. Techniques for extending the present work to include these features are discussed at the end of the paper.

2. Model formulation

We consider the advection–diffusion equation in one dimension. In a standard geopotential (or Cartesian) framework, this equation is

$$S_t + wS_z = -F^S_z, \qquad (2.1)$$

where w is vertical velocity, S is a tracer (read salinity), derivatives are taken in the Cartesian system, and F^S is the flux of tracer caused by unresolved scales of motion whose divergence locally affects tracer concentration. In a one-dimensional incompressible fluid, we append the constraint

$$w_z = 0 \qquad (2.2)$$

but allow w to be nonzero, envisioning boundary layers where needed to supply and absorb the associated mass fluxes.

A restatement of (2.1) in a quasi-Lagrangian framework, with vertical coordinate $\pi(x, y, t)$ and diacoordinate velocity w^{π} is

$$S_{t|\pi} + w^{\pi} S_z = -F_z^S, \tag{2.3}$$

where the temporal derivative is now taken in the quasi-Lagrangian coordinate system of a given π surface. [Note, we retain vertical derivatives with respect to z in (2.3), rather than fully transforming to a coordinate system using π as the vertical coordinate, because some of the analysis to follow is simpler to demonstrate in the fixed coordinate system.] The above may be derived by straightforward coordinate transformation. The vertical velocity of quasi-Lagrangian π surface is $(\partial z/\partial t)_{\pi} = w - w^{\pi}$. Aside from the requirement of monotonicity, the surface, π, and consequently the diasurface velocity, w^{π}, are at this point general.

The real ocean equation of state is a function of pressure and the two conservative tracers potential temperature and salinity. In this case, it is useful to employ the concept of neutral trajectories, which are those trajectories for which fluid parcels can be moved small distances without experiencing a gravitational restoring force. The dependence of the thermal expansion (α) and saline contraction coefficient (β) on pressure implies that these are not well-defined surfaces, although they may be unambiguously defined locally (McDougall 1987a). The latter point is relevant to this study as we work only in the vertical dimension.

There is a special choice for w^{π} that assures that the quasi-Lagrangian surface π is neutral, namely the choice

$$w^{\pi} = e \equiv \frac{-(\alpha F_z^{\theta} - \beta F_z^S)}{(\alpha\theta_z - \beta S_z)}, \tag{2.4}$$

where θ denotes potential temperature. In what follows, we reserve the symbol e for the dianeutral velocity, as distinct from the more general diasurface vertical velocity, w^{π}. Thus, fluid can pass through a neutral surface at the rate e determined by the small-scale diffusive processes. Equivalently, (2.4) ensures that the neutrality of the surface is preserved (McDougall 1987b).

a. *Flux properties*

To illustrate our generalization of mixing in layered coordinates, we choose to model all tracer concentrations as linear functions of depth within "layers," so that the fluid column in total is piecewise linear in tracer properties (see Fig. 1). This differs from the more standard representation for tracers in layered models, in which they exhibit discontinuities in value at interfaces and are considered "well mixed" vertically within each layer (see Bleck and Chassignet 1994). Finally, the procedure discussed here can be carried over to an arbitrarily smooth vertical representation for the tracers, although (certainly in our opinion) a point of diminishing returns is quickly realized, as will be seen.

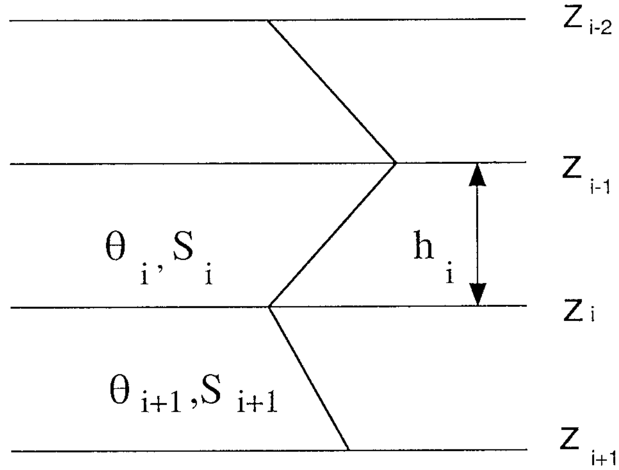

FIG. 1. Four interior "interfaces" or "joints" are presented. Tracer fields are assumed to be linear functions of depth. The tracers are assumed to be continuous, but their slope can change discontinuously at the interface joints. The diapycnal velocities at each interface are shown.

Twice vertically differentiating (2.1) within a layer shows that for linear tracer profiles the fluxes must be quadratic functions of height, z. Calculating the associated coefficients of the quadratics requires constraints, which we now examine.

If either (2.1) or (2.3) is now integrated over a small interval across a "joint" in the S profile, for example, between $z = z_i - \varepsilon$ and $z = z_i + \varepsilon$ in Fig. 1, there results (z is defined positive upward)

$$\begin{aligned} (\dot{z}_i - w)[S(z_i + \varepsilon) - S(z_i - \varepsilon)] + O(\varepsilon) \\ = F^S(z_i + \varepsilon) - F^S(z_i - \varepsilon) \quad \text{or} \\ -w^{\pi}\Delta[S] = \Delta[F^S] + O(\varepsilon), \end{aligned} \tag{2.5}$$

where $\Delta[X]$ represents the difference of property X when evaluated on either side of the joint, that is, at the height $z = z_i - \varepsilon$ just below the interface and at the height $z = z_i + \varepsilon$ just above the interface. Note that the identity $-w^{\pi} = (\dot{z} - w)$ has been used in (2.5). We now let ε tend to zero. Desiring continuous property profiles (i.e., $\Delta[S] = 0$) implies that the left-hand side of (2.5) is zero and thus that the diffusive property flux F^S must also be continuous.

Our desire to let real physical diffusive behavior shape our system as much as possible leads us to obtain a second constraint from (2.1). Differentiating that equation in z, interchanging the order of differentiation on the time derivative, and integrating in z over the joint eventually yields

$$\begin{aligned} [\dot{z}_i - w][S_z(z_i + \varepsilon) - S_z(z_i - \varepsilon)] \\ = F_z^S(z_i + \varepsilon) - F_z^S(z_i - \varepsilon) \quad \text{or} \end{aligned} \tag{2.6}$$

$$[\dot{z}_i - w]\Delta[S_z] = -w^\pi\Delta[S_z] = \Delta[F_z^S]. \quad (2.7)$$

Considering now other tracers, it is clear that we require

$$-w^\pi = \frac{\Delta[F_z^S]}{\Delta[S_z]} = \frac{\Delta[F_z^\theta]}{\Delta[\theta_z]} = \frac{\Delta[F_z^C]}{\Delta[C_z]}, \quad (2.8)$$

where C is any conservative tracer. The profiles, while linear in each layer, may differ in slope, making the above a nontrivial equation. This constraint is recognized as a generalization of one derived in McDougall and Dewar [1998, see Eq. (4) of that paper] for their discontinuous profiles to the present continuous property profiles with discontinuous first derivatives of both properties and fluxes. The above yields enough information to fully constrain the system.

In order to demonstrate how the scheme works, it is convenient to employ the same thought process as in McDougall and Dewar (1998) of regarding the vertical mixing to be localized in one layer at a time. The complete flux field of the model can then be constructed by summing the mixing contributions from each layer. This is analogous to solving the 1DADE with a Green's function technique, although the implementation described below differs slightly from this. Nonetheless, mixing is made fully at the disposal of the modeler in the sense that the diffusivities as a function of layer index can be imposed at the modeler's discretion and can also be functions of time.

Suppose that a nontrivial diffusivity is posed in a given interior layer (boundaries are considered later), we move to the computation of the fluxes directly required by that mixing. We now restrict the π surface to be neutral. Such a surface permits fluid to cross it only to the extent required by diffusive processes. The diasurface velocity of a neutral surface is given by $w^\pi = e$ as defined by (2.4).

First, note the mixing influence of a given layer extends beyond that layer. The simplest way to rationalize this comes from the requirement that e is well defined and continuous in the vertical. The formula (2.4) must then yield the same value for e regardless of the side of the joint where it is evaluated. Since in general $(\alpha\theta_z - \beta S_z)$ will be nonzero, nonzero flux divergences must then always exist on both sides of a joint neighboring an active layer, even in the extreme case of nontrivial mixing in one layer only. Thus, for an interior layer, we are faced with computing quadratic flux coefficients for one central and two neighboring layers. That is, there are up to four associated e's, namely the two at the joints bounding the central layer, and the two at the bounding interfaces z_{i-2} and z_{i+1} (see Fig. 1). The latter two are easy to dismiss by requiring flux divergences to vanish at the far interfaces, which implies $e_{i-2} = e_{i+1} = 0$. This has the welcome effect of localizing the *direct* impact of mixing in a given layer to that layer and its immediate neighbors. We emphasize direct here because we show below there is an indirect, global effect, caused by mixing in a given layer. This is a specific example of a general consequence of higher-order, smoother tracer representations; that is, the ''footprint'' of the mixing broadens. The vertical mixing stencil for the discontinuous tracer profile is one layer, while that for the linear approach is three layers. It can be shown that quadratic tracer profiles require five layers to determine all the associated coefficients. It is in this sense of broadening footprints and the rapid growth of algebraic complexity in writing the constraints that we have found the diminishing returns of higher-order approximations in layered coordinates.

Thus, for piecewise linear tracer profiles and nonzero mixing in layer i, there are two sets of nine coefficients (the quadratic coefficients for θ and S in layers i, $i + 1$, and $i - 1$) and two dianeutral velicities, e_i and e_{i-1}, yielding 20 unknowns. These may be reduced by four due to the requirement of vanishing flux divergences for θ and S at z_{i-2} and z_{i+1}, and by four again by requiring zero flux of θ and S at those interfaces. Requiring continuity of tracer flux at the interfaces z_i and z_{i-1} [see (2.5)] leaves eight unknowns. At this point in the analysis, the flux fields associated with mixing in a given layer can be written, without loss of generality, as

$$F_{i-1}^{C,i} = a_{i-1}^{i,C}(z - z_{i-2})^2/2, \quad (2.9)$$

$$\begin{aligned} F_i^{C,i} = {} & (a_{i+1}^{i,C}h_{i+1}^2 + a_{i-1}^{i,C}h_{i-1}^2 - F_i^C)(z - \overline{z}_i)^2/h_i^2 \\ & + (a_{i-1}^{i,C}h_{i-1}^2 - a_{1+1}^{i,C}h_{i+1}^2)(z - \overline{z}_i)/(2h_i) \\ & + F_i^C, \quad \text{and} \end{aligned} \quad (2.10)$$

$$F_{i+1}^{C,i} = a_{i+1}^{i,C}(z - z_{i+1})^2/2, \quad (2.11)$$

where the superscript C denotes tracer (either θ or S), the superscript i denotes the layer in which the mixing effect originates, and the subscript i, $i + 1$, or $i - 1$ the layer in which the mixing effect is occurring. Note that (2.9) and (2.11) satisfy the no flux and no flux divergence constraints on the far interfaces, z_{i-2} and z_{i+1}. This is illustrated in Fig. 2c, where the flux profile of mixing in layer i is illustrated. The quantity $\overline{z}_i$ denotes the central depth of layer i,, and evaluation of the above at z_{i-1} and z_i confirms that the fluxes are continuous. The eight unknowns are $a_{i+1}^{i,C}$, $a_{i-1}^{i,C}$, F_i^C for $C = \theta$ and S (six total), e_{i-1}^i, and e_i^i. Generalizations of the above apply near the boundaries.

Two of the constraints necessary to determine the remaining coefficients are given by (2.7) (for salinity only) for the two bounding interfaces. We then apply (2.4) at each interface for another two constraints. Requiring e_i to be the same regardless of which side of the interface (2.4) is evaluated yields two further constraints and also guarantees that the potential temperature field satisfies a constraint like (2.7). [Equivalently, one can apply (2.4) just once at each of the two joints (say just above a joint) and apply (2.7) to both θ and S at each of these two joints.] This leaves two remaining

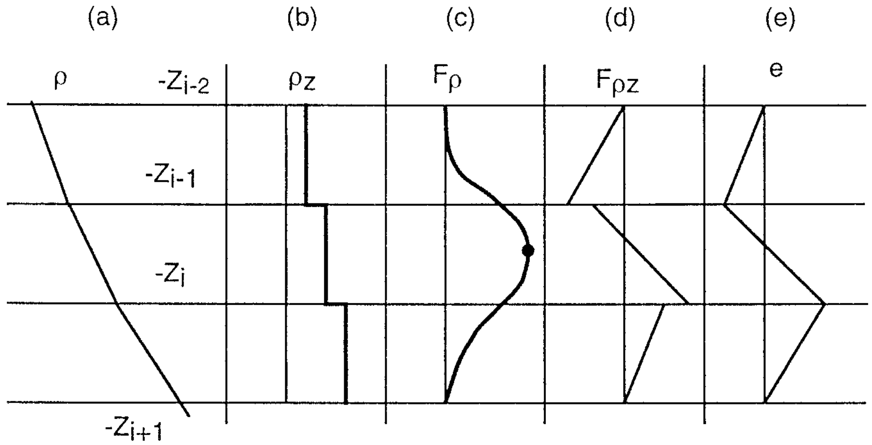

FIG. 2. Flux structure for a given interior flux magnitude. The density is continuous, but the density gradient changes discontinuously at interfaces z_{i-1} and z_i. Moving left to right, (a) ρ, (b) ρ_z, (c) flux, (d) flux divergence, and (e) entrainment are shown. The magnitude of the central flux is denoted by the circle in (c). Note fluxes are continuous, although flux divergences are not. The zero in the flux divergence occurs at the maximum of the flux, and neither needs to occur at the layer middle. Fluxes and entrainments vanish at z_{i+1} and z_{i+2}.

degrees of freedom that we set by specifying a flux magnitude, F_i^C, appropriate to the layer middle depth $\overline{z}_i$, one for each of θ and S. The form of the flux field generated by this procedure is depicted schematically in Fig. 2. Here it is assumed S is uniform but that θ is not, that is, that the fluid is stratified in one property only. Again, we emphasize that the flux field generated by an imposed flux at $\overline{z}_i$ comes as a ''triple,'' that is, as a flux in three layers. The density flux field so required, some derivatives and e are plotted in Figs 2a–e. The flux magnitude, F_i^C, appears in Fig. 2c as the large solid dot, and the direct mixing onsequences of this one imposed flux at $\overline{z}_i$ in layers i, $i + 1$, and $i - 1$ are shown. Note that the far-field entrainments, e_{i+1} and e_{i-2}, vanish, as do the fluxes and flux divergences at the interfaces z_{i+1} and z_{i-2}. The flux divergence vanishes at the same depth as the maximum in flux, which does not necessarily occur at the layer center, $\overline{z}_i$.

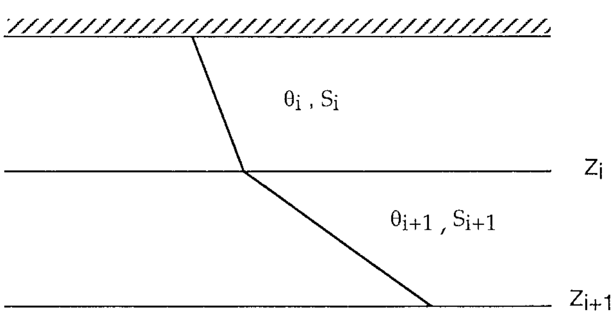

FIG. 3. Boundary conditions. Entrainment e is used as a constraint at z_i, but diagnosed at the boundary. For the layer adjacent to the wall, either fluxes or tracer values can be specified, depending on the boundary conditions.

b. Boundaries

The procedure for the interior is modified slightly for layers neighboring boundaries (see Fig. 3). The main reasons for these modifications are that boundary constraints provide information about fluxes not available in the interior.

Thus at a boundary, after the constraints of locality and continuity of flux have been employed, there remain seven unknowns for S and θ. Two of them are removed by asserting a flux magnitude for each tracer at the layer center. We then apply (2.7) and the formulas for e_i to leave two unknowns. For Neumann conditions (e.g., insulating boundaries) these constraints act directly on the flux values. Since the constraints on the fluxes of the neighboring layers include that the fluxes $F_{i+1}^i = 0$ (for the bottom) or $F_{i-1}^i = 0$ (at the top), the flux constraint operates directly on the boundary layer flux magnitude. For Dirichlet conditions, the two constraints are set on the boundary layer flux divergences for the same reason. In both cases, the system is closed.

Note also, the boundaries represent special coordinates of the model, in that they do not in general obey a quasi-Lagrangian constraint. One ramification of this is that the tracer behavior on boundaries need not be neutral. Thus, the end state of a column of fluid subject to insulating boundary conditions is that it be uniform in potential temperature and salinity, the values of which are known from heat and salt conservation. This final state is unique, a feature that represents an improvement over the behavior expected from classical layered models where the final state in an insulating box generally consists of two layers whose θ and S depend on the mixing history (see Fig. 5b of McDougall and Dewar 1998).

Another ramification is that boundary information can flow into the interior. To see this, consider the kinematic equation describing fluid movement at the boundary:

$$\dot{z} = w - e. \tag{2.12}$$

Recall, by definition, e can be computed anywhere in the fluid. The procedure described above generates a flux field everywhere, in particular at the boundaries, and the assumed form for the tracer fields implies e at a boundary can be computed. Suppose we consider $w > 0$ and confine our interests to the lower boundary where, for Dirichlet conditions, θ is specified. If $\dot{z}$ from (2.12) is negative, we conclude diffusive effects overwhelm advective effects and the calculation proceeds as described above. On the other hand, if (2.12) implies $\dot{z}$ is positive, the boundary points must be allowed to flow into the domain. This results in an extra layer being formed against the bottom boundary with $\theta_z = 0$. This will be seen in the transient Munk problem discussed below, and the switch from the former to the latter condition occurs when (2.12) passes through zero.

c. Local constraints on mixing and global effects

The calculation of the flux magnitude, F_i^C,[1] of a given layer is a rather subtle affair, and introduces a global character to mixing, in spite of the application of local mixing parameterizations in the center layer of each triple. This behavior occurs because the total flux in a given layer comes from three contributions: one from the central layer and one each from the neighboring layers given the three-layer footprint of the direct effect of mixing. We wish to constrain the flux of tracer in a given layer by using the local tracer gradient and the layer diffusivity coefficient; in all examples quoted here, we will use

$$F_{\text{total}}^{C,i} = -K_{\nu,i} C_z^i, \tag{2.13}$$

where C again denotes the tracer (e.g., salinity, potential temperature, or Freon). We apply (2.13) to the middle height, $\overline{z}_i$, of the layer in question. Note that this guarantees the physically desirable properties of downgradient fluxes at the layer center and that the total mixing flux is determined purely by local properties of the fluid. On the other hand, the three-layer footprint of the present approach implies that (2.13) has a global impact.

Consider the simple case where the fluid is stratified in one tracer only, say S; a linear equation of state is assumed; and the interior layers possess equal salinity (and hence density) intervals. Calculating the coefficients reveals that the total flux in layer i at the layer center is then

$$F_{\text{total}}^{S,i} = F_i^S + \frac{F_{i+1}^S}{6} + \frac{F_{i-1}^S}{6}. \tag{2.14}$$

The quantities F_{i+1}^S and F_{i-1}^S are the so-called flux magnitudes associated with the flux triplets centered in layers $i + 1$ and $i - 1$. Applying (2.13) to each layer yields a tridiagonal matrix equation, the solution of which may be obtained via a direct solver. The case of unequal density intervals is only slightly more involved with the coefficients becoming non constant and time dependent, rather than being simply 1 or $\frac{1}{6}$. In any case, the calculation of the required flux magnitudes involves the solution of a tridiagonal matrix equation. Thus, the flux magnitudes F_i^C in each layer are known and the complete set of coefficients and interface dianeutral velocities may be calculated.

However, the solution discussed above is global in that the inversion of the tridiagonal matrix implies far-field effects. In Fig. 4a, we display flux magnitudes for the specific Green's function approach described above. The flux magnitudes are properties of the layers, and not continuous functions of depth, so we have adopted a block presentation in this figure. In this experiment, the system consisted of 11 layers of 200-m thickness each. The fluid was stratified in θ only with equal temperature intervals of 1.95°C across each layer. In all but layer 6, the diffusivity coefficient, $K_{\nu i}$, was assumed to vanish. In layer 6, the diffusivity was assigned a value of 2×10^{-4} m^2 s^{-1} and the resulting tridiagonal matrix equation for the flux magnitudes solved. Note the appearance of nontrivial flux magnitudes in the layers neighboring layer 6. In fact, nonzero flux magnitudes occur in all layers due to the presence of mixing in layer 6, but the amplitudes of the fluxes decrease as one moves away from the active layer. The reason for the far-field flux magnitudes is the requirement from (2.13) that total flux in layers other than 6 identically vanish and the fact that the flux magnitudes shown in Fig. 4a have associated with them a continuous flux profile spread over a triplet. So, for example, there is a flux contribution in layer 5 from layer 6. To cancel this flux at layer center, a nonzero flux magnitude is required in layer 5. This then generates a flux contribution in layer 4, the cancellation of which requires a nonzero flux magnitude in layer 4, and so on. These flux magnitudes, necessary to ensure zero total flux at all layer centers aside from 6, appear in Fig. 4a.

Of course, these flux magnitudes do not constitute the entire flux picture in this problem. That is controlled by total flux, which is a smooth function of z, and we present a picture of total flux in Fig. 4b. This flux field is the true Green's function flux field for mixing in layer 6 only. The total flux in each interior layer is the sum of the contributions from the central layer and its two neighbors. The center depth of each layer is denoted by a circle, and the interfaces between the layers are denoted by the horizontal lines. Note that aside from the middle layer, where mixing is active, the total flux van-

[1] We use the term flux magnitude to denote the flux value assigned at the middle of the central layer of a given triple. This will differ in general from the total flux in that layer.

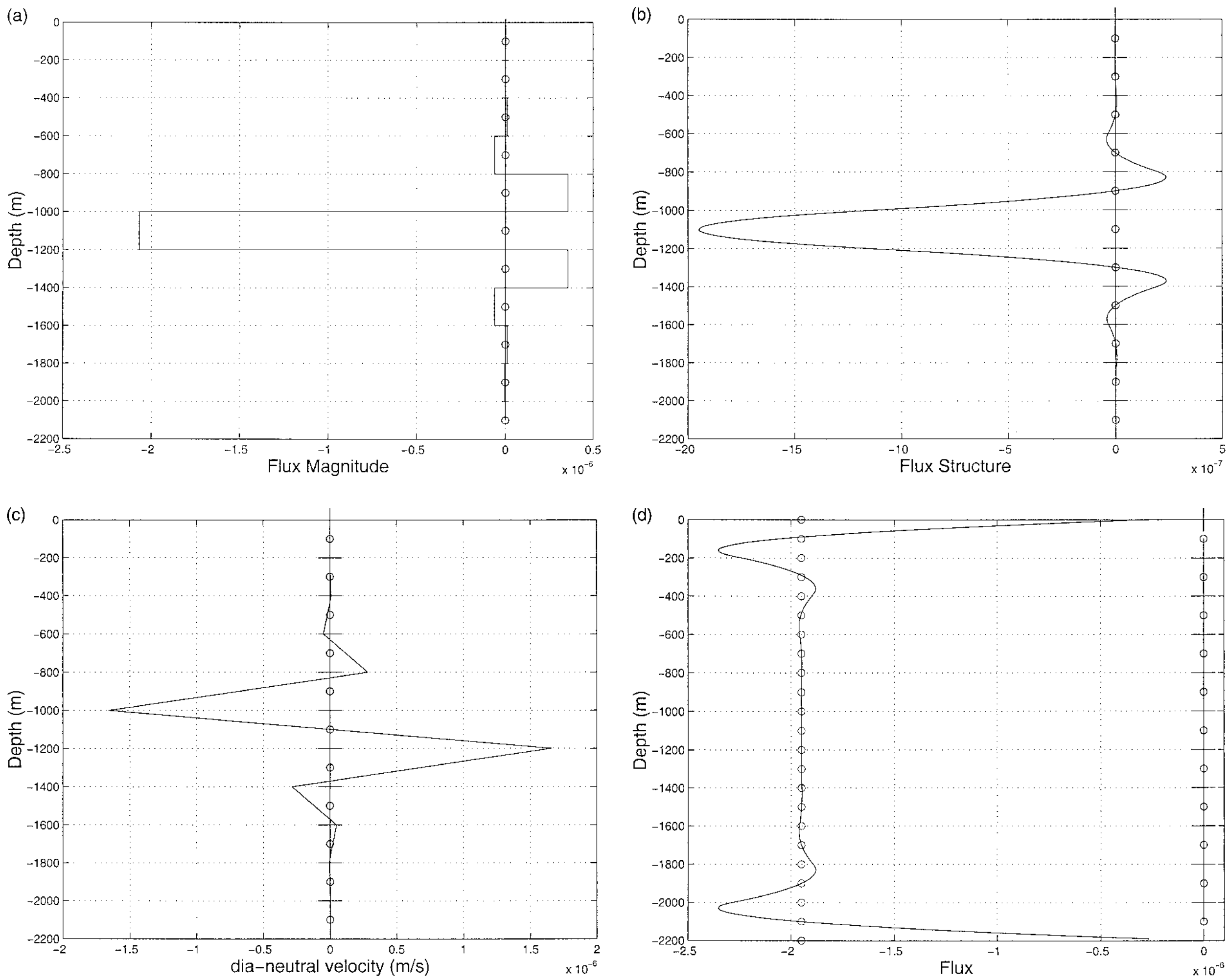

FIG. 4. (a) The set of flux magnitudes, F_i^s, generated by mixing in layer 6 of an 11-layer model. The circles denote the central depth of the layers and the horizontal lines the joints or interfaces between piecewise linear tracer profiles. The total flux field, formed by summing the flux contribution to a layer from the central and neighboring layers, generated by the flux magnitude field in (a) is shown in (b). This flux field corresponds to the Green's function generated by mixing in layer 6 only. Note the total flux at the central depth in all layers except 6 vanishes. (c) The diapycnal velocity field for this problem. Note the discontinuities in slope of the *e* profile occurring at the interfaces. The reconstructed flux for uniform vertical diffusivity appears in (d). This flux field was built by summing flux footprints like that shown in (b). Such footprints were built using single nonzero diffusivities in each layer. The interior flux is consistent with a uniform value for the diffusivity, in spite of the requirement that the diffusivity be imposed at the center of each layer only. Near the boundaries, a Gibbs phenomenon sets in and generates some wiggles.

ishes at layer center. The total flux field does oscillate, generating in this case positive values in neighboring regions, these representing local upgradient fluxes. But, the fact that each of these is bounded on both sides by zero flux values confines these fluxes in influence; their role is to maintain linear tracer profiles. Also, the amplitude of the total flux decreases away from the active mixing layer, leading us to conclude this indirect, global effect of mixing, while present, is weak.

The diapycnal velocities generated by the Green's function flux field in Fig. 4b appear in Fig. 4c, where the circles and horizontal lines play the same role as previously. The largest *e*'s, by far, are those bounding the active layer. A rapid dropoff moving away from layer 6 is noted. The diapycnal velocity is continuous and linear in each layer, as required for linear tracer profiles. The asymmetry of the *e* field reflects the mixing in the central layer only.

d. Effective diffusivity

A question of some interest is the effective diffusivity generated by this scheme. The motivator for this question comes from the fact that diffusive fluxes throughout the fluid column, while smooth and continuous, are constrained by specified diffusivity coefficients at a finite number of locations. Away from those locations, the local diffusivity coefficients can change value and even become negative, as shown in Fig. 4b. It is not a priori obvious how the resultant effective diffusivity compares to the explicitly applied diffusivity. We here argue that the two are identical.

The evidence for this comes from Fig. 4b, where the properties of the flux field generated by mixing in a single layer were illustrated. Consider the vertical integral of the flux shown in Fig. 4b over the entire water column. To estimate an effective diffusivity, this integral was equated to that which would be obtained by integrating the flux generated by a constant diffusivity in layer 6 surrounded by vanishing diffusivities elsewhere. This yields

$$\int_{-H}^{0} F^C(z)\, dz = -K_{\nu,\mathrm{eff}}\delta C,$$

where δC is the total tracer change across layer 6 and F^C is the flux in Fig. 4b. Evaluating this formula resulted in $K_{\nu,\mathrm{eff}} = 2 \times 10^{-4}$ m^2 s^{-1}, which is identical to the diffusivity imposed on layer 6 at the central depth.

Similar flux footprints for nonzero diffusivities in individual layers were computed for every layer of the profile discussed in Fig. 4. In these runs, the employed diffusivity value was set to $K_\nu = 2 \times 10^{-4}$ m^2 s^{-1} for every layer. These fields were then summed to construct the flux field, which, in theory, should model that associated with a uniform value for the vertical diffusivity of $K_\nu = 2 \times 10^{-4}$ m^2 s^{-1}. The results of this exercise are shown in Fig. 4d, where it is seen that the interior of the fluid consists of a nearly uniform flux consistent with the specified diffusivity and the imposed tracer profile. Near the boundaries, the flux deviates from a uniform value, displaying some wiggles reminiscent of a Gibbs phenomenon. This reflects the no flux boundary conditions operating right at the walls, in conjunction with the finite flux imposed at the center of the boundary layers. This finitely resolved model cannot perfectly model continuous structure, so the flux field exhibits some near-boundary variability.

In the event that the fluid is stratified in both θ and S, more effort must be expended to compute the flux magnitudes. For a linear equation of state and equal density intervals across layers, essentially two tridiagonal matrices must be solved. In this case, a buoyancy ($-\alpha\theta + \beta S$) variable can be formed, and the equations governing it are identical to those for a fluid stratified in one tracer only. Thus, manipulating the coefficient equations eventually yields the result that

$$\frac{3}{4}[\alpha a^{i,\theta}_{i+1}h^2_{i+1} - \beta a^{i,S}_{i+1}h^2_{i+1}] = \frac{3}{4}[\alpha a^{i,\theta}_{i-1}h^2_{i-1} - \beta a^{i,S}_{i+1}h^2_{i+1}]$$
$$= \alpha F^\theta_i - \beta F^s_i \qquad (2.15)$$

from which it is seen that the layer density flux magnitude, $F^\rho_i = -\alpha F^\theta_i + \beta F^s_i$, is subject to the constraint

$$F^\rho_i + \frac{F^\rho_{i+1}}{6} + \frac{F^\rho_{i-1}}{6} = -\alpha K_{\nu,i}\theta_{iz} + \beta K_{\nu,i}S_{iz}. \qquad (2.16)$$

If the density steps across layers are not all equal, the form of the matrix is still tridiagonal, but somewhat more algebraically complex. The matrix equation for the density flux is calculated from the known diffusivities and tracer fields. The density flux magnitude, $F^\rho_i = -\alpha F^\theta_i + \beta F^s_i$, within each layer is then known and the diapycnal velocities, e_i, can be computed. Consider then the equations for the fluxes of one of the two tracers, say S. There are two unknown coefficients and an unknown tracer flux magnitude in the quadratic formulas for the flux [see (2.9)–(2.11)]. Given knowledge of e_i, (2.8) applied at z_i and z_{i-1} provides two constraints from which the coefficients can be written in terms of the unknown tracer flux magnitudes. This leads to a second tridiagonal equation for the S flux magnitudes constraining the total F^S flux at layer centers according to (2.13). Once these are known, the other tracer flux magnitude, F^θ, can be computed from the known density fluxes computed in (2.15).

If a real equation of state is used, a simple buoyancy variable cannot be formed, and the matrix equation governing the flux magnitudes does not collapse to a tridiagonal. Rather, it generally is a seven-diagonal matrix (the main diagonal plus the three neighboring diagonals on either side), which, while sparse, must be solved using iterative methods. Once the flux magnitudes are known, calculating the diapycnal velocities and coefficients for both tracers is straightforward.

Note also that the mixing of other passive tracers (e.g., Freon, CO_2, etc.) can be computed immediately given the above procedure. The only substantive difference is that the dianeutral fluxes e_i are not considered as unknowns; rather, they are specified by the above solution. Then, the flux field associated with the mixing in a layer is quickly reduced to three unknowns, given the requirements of flux continuity and locality. Applying a condition like (2.8) at the interfaces provides two constraints, and a third comes from (2.13).

3. Examples

Here we provide some examples of the above procedure. In the first two, we solve two equations like (2.1) for salinity and potential temperature, subject to the constraint that the system evolves in piecewise linear fashion. The joints evolve neutrally and the spatial representation of the system is exact. The system of equations necessary to fully specify the flux coefficients was solved numerically by LU decomposition and the system was time stepped by a fourth-order Runge–Kutta method. In the third, we work with a fluid stratified in temperature only. In all cases, we have for simplicity used a linear equation of state.

a. Neumann conditions

First, we demonstrate the evolution of a system in an insulating box. This appears in Fig. 5, where several

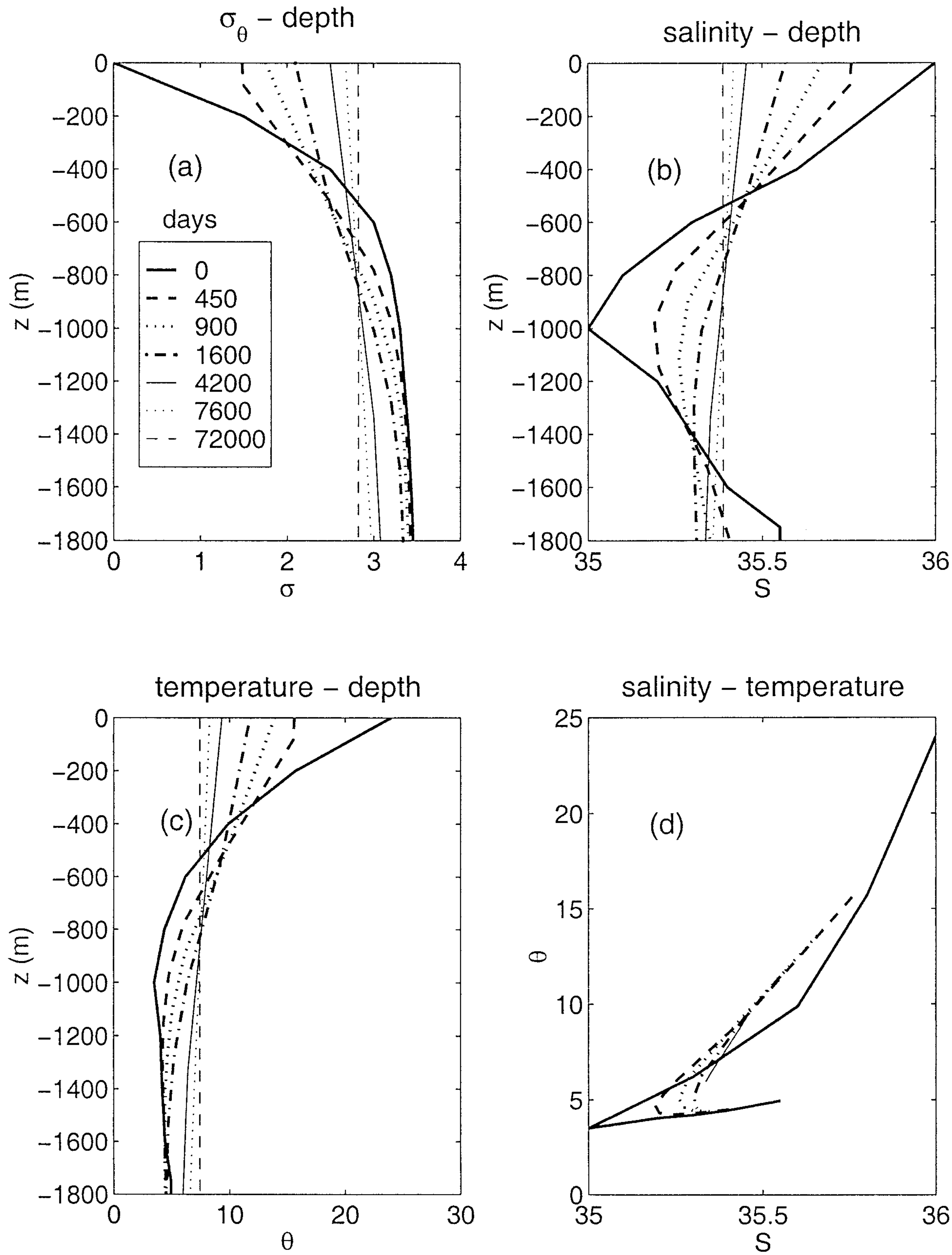

FIG. 5. Diffusive evolution for an insulated 1800 m deep column of water is shown. The vertical diffusivity for both S and θ are 1×10^{-3} $m^2\ s^{-1}$. Several physical space profiles from various instants in time are shown in (a) for ρ, (b) for S, and (c) for θ. The S–θ plane evolution appears in (d). The time in days associated with the traces appears in the legend in (a). The system eventually relaxes to a well-mixed state.

density, θ and S profiles appear in panels a, b, and c, respectively. The water column in this example is 1800 m deep, 10 layers are involved, and the diffusivities are uniform at 1×10^{-3} m^2 s^{-1}. This is somewhat more diffusive than open ocean observations would support for the real ocean (Ledwell et al. 1992). The several traces come from various points in time during the experiment. The legend in Fig. 5a denotes the time in days of each profile. The last trace, which shows virtually uniform θ and S, comes after a little less than 200 yr of model time.

The S–θ diagram representation of these experiments appears in Fig 5d. Again, the several traces correspond to different points in time from the experiment, but match the physical space traces in the earlier plots. These traces demonstrate the capacity of this scheme for removing curvature in the S–θ plane that, in turn, is a trait required of a physically based mixing scheme.

b. Dirichlet conditions

Here we recreate the classical Munk abyssal recipes solution (Munk 1966). This solution assumes the thermocline is generated by a balance between upwelling and the downward diffusion of buoyancy in a purely one-dimensional sense. The abyssal and surface properties are assumed fixed (Dirichlet conditions) and a nondivergent vertical velocity field is specified. A sequence of states from an initial value run is shown in Fig. 6. This experiment employed a fluid of 1800-m depth, 11 layers, a constant diffusivity value of 2×10^{-4} m^2 s^{-1} and an upwelling value of 2×10^{-6} m s^{-1}.

The θ, S, and density profiles appear in Figs. 6a–c and the S–θ plane evolution appears in Fig. 6b. The time in days corresponding to the traces appears in the legend in Fig. 6a. The boundary layer formation characteristic of the thermocline appears in the later stages of the experiment in Figs. 6a–c. At the same time, the S–θ plane demonstrates the tendency for the system to obtain linear tracer profiles. The latter is expected since mixing is expected to remove curvature in the S–θ plane.

c. A comparison of adaptive and fixed grid methods

The traces appearing in Fig. 7 are solutions of the Munk problem for a fluid stratified in temperature only. A fluid of 2000-m depth was assumed and 11 layers were involved in the generation of the quasi-Lagrangian solutions. The upper 500 m only are shown in Fig. 7a and the entire water column in Fig. 7b. Equal density intervals were assigned to each layer and the initial conditions consisted of a linear density profile. The diffusivities were set to 2×10^{-4} m^2 s^{-1} and the upwelling vertical velocity to $w = 2 \times 10^{-6}$ m s^{-1}. We show final state profiles for temperature, from which the boundary layer at the top is evident. Here we compare four solutions in order to illustrate some advantages provided by the quasi-Lagrangian approach. One of these solutions was generated using a high-resolution fixed grid. Specifically, 51 points were included in the vertical, yielding a resolution of 40 m per layer, a thickness characteristic of highly vertically resolved numerical experiments. The solution so generated is essentially identical to the analytically expected solution, as other tests have shown, and is plotted in Figs. 7a,b as a dashed line. The solution obtained using the current piecewise linear quasi-Lagrangian method is plotted in Figs. 7a,b using a solid line. With the exception of the 250–450-m range, these two are essentially indistinguishable.

The third solution shown has been generated using the approach advocated in McDougall and Dewar (1998), in which the density field is represented by a discontinuous profile. The mixing scheme is as outlined in that paper. A total of 10 layers were used and the diffusivity coefficients and vertical velocities are identical to those in the previous two cases. Note that the comparison between this profile and the first two is quite satisfactory, although the rms difference between this case and the true solution is larger than that between the piecewise linear solution and the true solution. This is to be expected given that a higher-order representation of the tracer fields has been assumed in the construction of the latter.

Finally, we also show the solution generated using second-order central differencing on a fixed grid consisting of 11 points in the vertical (dotted line). Note, in a crude sense, the ''resolution'' of the fixed grid and that of the quasi-Lagrangian grid is the same, in that essentially the same number of degrees of freedom occur in the latter three cases. The comparison between this discrete solution and the correct underlying solution is however in this case the least satisfactory. Note that the latter solution consists of a constant temperature, equal to the imposed bottom temperature, until the last interior grid point. The thermocline in this solution then occurs only in the top grid box, where the entire transition to the imposed surface temperature takes place. The rms difference between this solution and the underlying correct solution is the largest of the three considered solutions.

One may argue that we have biased against the Cartesian approach in our comparison by using a uniformly spaced grid, rather than, say, one with the highest resolution near the surface and lowest near the bottom. We offer the following points in relation to this issue. First, uniform grids like those applied here are simple and second-order accurate. To obtain second-order accuracy with nonuniform grids requires more numerical overhead. Second, recall that our quasi-Lagrangian approaches are also unbiased, in that we chose to divide the fluid into equal density intervals in order to define our layers. In this sense, we are comparing like models, inasmuch as we can make such a statement. Had we chosen unequal grid intervals for the finite-difference approach, a comparison between comparable methods would have allowed us freedom in our choice of layer

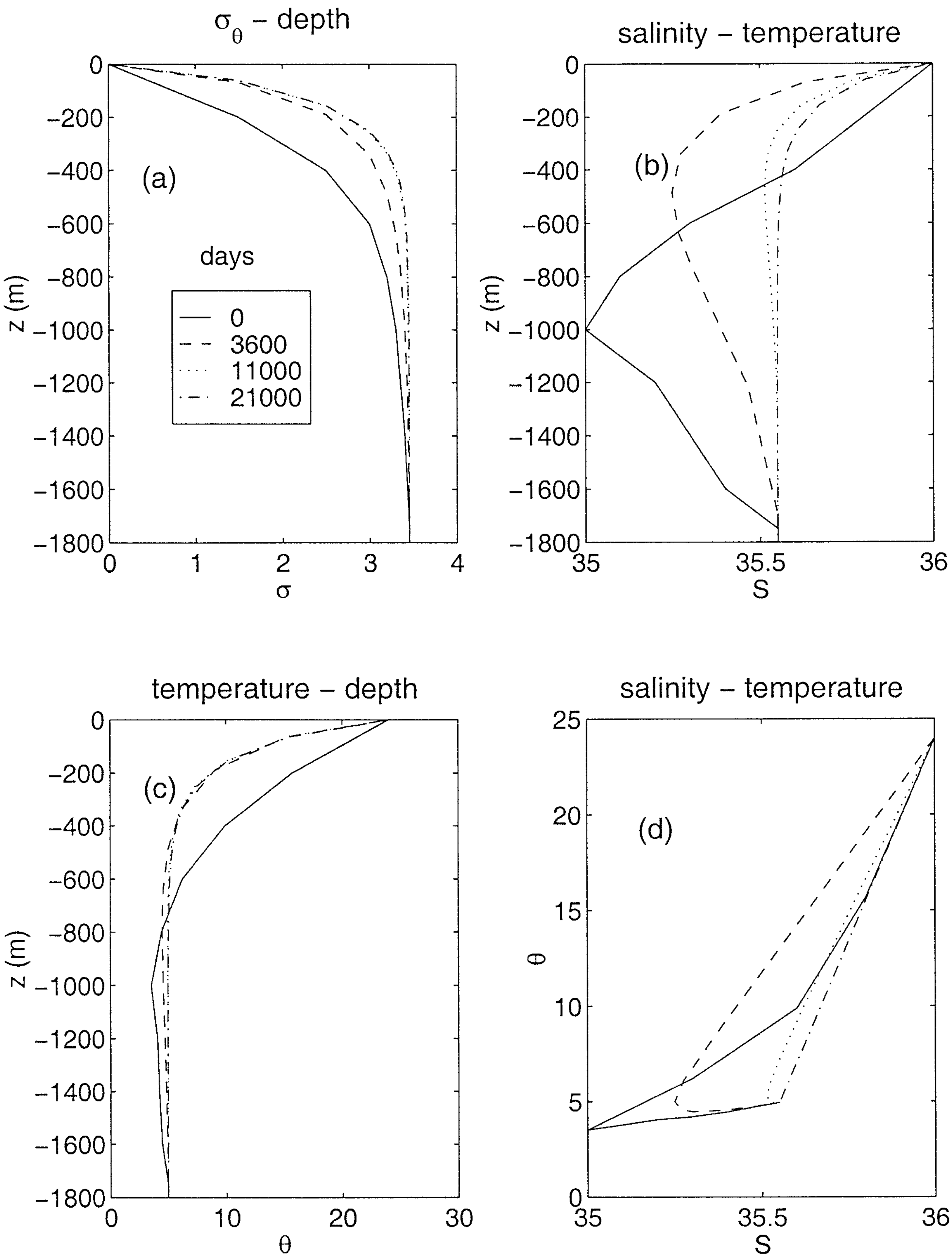

FIG. 6. The Munk problem for a 1800 m deep fluid. Vertical velocity $w = 2 \times 10^{-6}$ m s^{-1} throughout the water column and vertical diffusivity was uniform at $K_v = 2 \times 10^{-4}$ m^2 s^{-1}. Physical space tracers appear for ρ in (a), S in (b), and θ in (c). Evolution in the S–θ plane appears in (d). The time in days associated with each trace is given in the legend in (a).

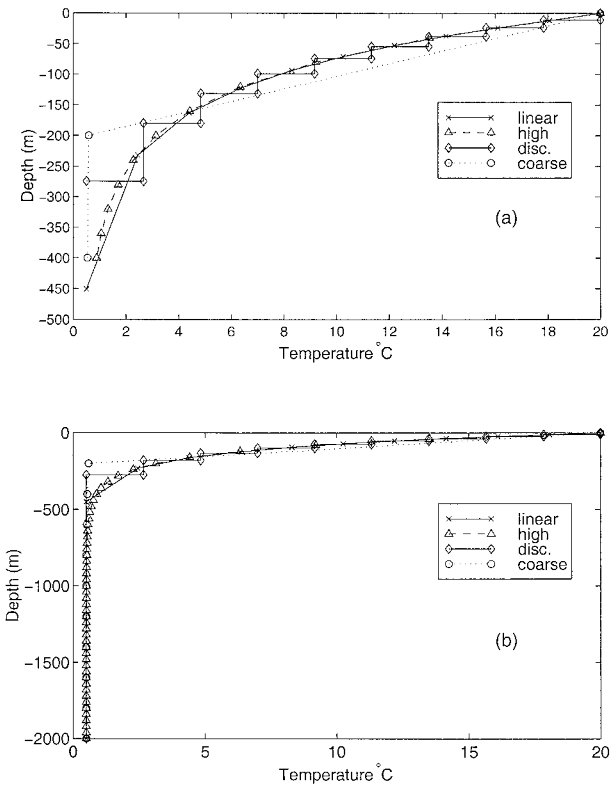

FIG. 7. Four numerically generated solutions to the steady-state Munk problem are compared: (a) the upper 500 m and (b) the whole water column. The fluid is 2000 m deep, $K_{\nu i} = 2 \times 10^{-1}$ m^2 s^{-1} and $w = 2 \times 10^{-6}$ m s^{-1}. The dashed line (labeled high) comes from a second-order-accurate finite-difference solution with 51 grid points ($\delta z = 40$ m). This trace is essentially indistinguishable from the analytically expected solution. The smooth solid line (labeled linear) was generated using the piecewise linear quasi-Lagrangian approach developed in this paper. Eleven layers were used. The trace so generated is very close to the previous solution. The discontinuous solid line (labeled disc) was generated using the lower-order quasi-Lagrangian approach developed in McDougall and Dewar (1998), and the dotted line (labeled coarse) was generated by second-order finite-difference approach using 11 grid points ($\delta z = 200$ m).

density intervals. One may then always contend that we have not chosen the optimum set of unequal intervals for either the density or spatial grid. We have avoided all these ambiguities in our choice of the simplest set of grid spacings. Finally, we point out that we know the solution of this particular Munk problem. A choice of fine grid intervals near the surface reflects this knowledge. We do not however generally enjoy this luxury, and in a time-dependent ocean model, any particular spatial grid choice cannot be defended a priori as the best one for all the flow dynamics that the model is likely to generate. As demonstrated here, even a quasi-Lagrangian grid not especially optimized for a given problem can be expected to adapt surprisingly well to the details of the solution.

The point of the previous comparison is that quasi-Lagrangian solutions, like those proposed here, represent very efficient methods for obtaining accurate solutions to the governing equations of fluid mechanics. The above comparisons suggest accuracies of the quasi-Lagrangian solutions are competitive with those of second-order fixed gridpoint schemes having five times the spatial resolution. This advantage is considerable given that the computer power of the foreseeable future will remain a limiting factor on the size of ocean climate models.

4. Discussion

We have proposed a method for solving the advection–diffusion equation that generalizes the approach classically taken in layered models. There it is envisioned that the fluid is composed of several well-mixed layers with step discontinuities in properties at the interfaces. The advantages of this layered approach are that exact information about the tracer profiles throughout the water column is available, the solution suffers no spatial truncation, and the scheme is quasi-Lagrangian. The weakness of the standard layered approach is phenomenological, in that the ocean does not consist of a series of well-mixed layers.

Here we retain all the above advantages while attacking the disadvantage by in effect constructing a higher-order scheme. Tracer profiles are modeled as linear functions of depth and the structure of the flux field consistent with this is determined. We are able to build into this scheme the properties of overall downgradient diffusion, neutral behavior, and preferential reduction of curvature in the S–θ plane. Examples using Neumann and Dirichlet boundary conditions have been shown. In principle, the methods proposed here can be generalized to tracer profiles with discontinuities dismissed to derivatives of arbitrarily high order. The cost of this is an increasing mixing footprint. For example, quadratic tracer profiles with continuous first derivatives and discontinuous second derivatives involve a flux pattern in five layers and, for a linear equation of state, the solution of a pentadiagonal matrix to compute the layer flux magnitudes. Nonlinear equations of state involve broader matrices.

We stress that many issues require consideration before these ideas can be incorporated into a working three-dimensional model: among these are the inclusion of along-surface advection and the joining of the interior to the mixed layer. Regarding the latter topic, there do seem to be some promising avenues. The single modification to the procedure outlined here is that the tracer values on the boundary joints should be constrained to remain on their initial density surface, rather than to evolve nonneutrally. This has the disadvantage of removing the uniqueness of the solution allued to in section 2, but only near the boundaries. The advantage is arbitrary heat and salt fluxes and surface mixing models can be accomodated. With regard to the former problem, a promising approach is to match a well-mixed layer in momentum to the described tracer model. Advection terms in the tracer equations are then consistent with the linear temperature profile, and a single mixing stress term appears in the momentum equations.

A separate issue is that layered coordinates in general develop regions where the thickness of the layers becomes very small. This presents a time-stepping problem as very thin layers require very small time steps for stability when explicit schemes are used. Implicit schemes do not suffer from this constraint and are therefore to be preferred. A difficulty with implicit methods of the present procedure is that it is nonlinear in the layer thicknesses. Hallberg (2000) has recently addressed this issue for the case of well-mixed layers and the McDougall and Dewar (1998) scheme. It appears that his methodology migrates to this scheme as well; thus, providing an implicit time-stepping procedure for this layer representation.

We feel the potential for this representation to yield an improved vertical tracer representation in numerical models provides adequate motivation for work in these areas. On the other hand, this approach can be used now in inverse models, whose dynamics are represented by geostrophy.

Acknowledgments. This work was begun while the authors were visiting the Institut für Meereskunde in Kiel, Germany, and it is a pleasure to acknowledge the hospitality of that institution as well as the many interesting conversations on this topic with our host, Prof. Jürgen Willebrand. T.J.McD. would also like to thank the Alexander von Humboldt Foundation for generously supporting his visit to Germany through a research award. The figures were prepared by Sheila Derby. Ms. Jane Jimeian assisted with several computational tasks. WKD is sponsored by NSF Grant OCE-9617728 and NASA Grant NAG5-4813. This work is a contribution to the CSIRO Climate Change Research Program.

REFERENCES

Bleck, R., and D. Boudra, 1981: Initial testing of a numerical ocean circulation model using a hybrid (quasi-isopycnic) vertical coordinate. *J. Phys. Oceanogr.,* **11,** 755–770.
——, and E. P. Chassignet, 1994: Simulating the oceanic circulation with isopycnic-coordinate models. *The Oceans: Physical–Chemical Dynamics and Human Impact,* S. K. Majumdar et al., Eds., The Pennsylvania Academy of Science, 17–39.
Bryan, F., 1987: Parameter sensitivity of primitive equation ocean general circulation models. *J. Phys. Oceanogr.,* **17,** 970–985.
Gent, P., and J. McWilliams, 1990: Isopycnal mixing in ocean circulation models. *J. Phys. Oceanogr.,* **20,** 150–155.
Griffies, S., A. Gnanadesikan, R. Pacanowski, V. Larichev, J. Dukowicz, and R. Smith, 1998: Isoneutral diffusion in a *z*-coordinate model. *J. Phys. Oceanogr.,* **28,** 805–830.
——, R. Pacanowski, and R. Hallberg, 2000: Spurious diapycnal mixing associated with advection in a *z*-coordinate ocean model. *Mon. Wea. Rev.,* **128,** 538–564.
Hallberg, R., 2000: Time integration of diapycnal diffusion and Richardson number–dependent mixing in isopycnal coordinate ocean models. *Mon. Wea. Rev.,* **128,** 1402–1419.
Hirst, A. C., and T. J. McDougall, 1998: Meridional overturning and dianeutral transport in a *z*-coordinate ocean model including eddy-induced advection. *J. Phys. Oceanogr.,* **28,** 1205–1223.
Hu, D., 1996: The computation of diapycnal diffusive and advective scalar fluxes in multilayer isopycnic-coordinate ocean models. *Mon. Wea. Rev.,* **124,** 1834–1851.
Ledwell, J., A. Watson, and C. Law, 1992: Evidence for slow mixing across the pycnocline from an open-ocean tracer-release experiment. *Nature,* **364,** 701–703.
McDougall, T. J., 1987a: Neutral surfaces. *J. Phys. Oceanogr.,* **17,** 1950–1964.
——, 1987b: Thermobaricity, cabbeling and water-mass conversion. *J. Geophys. Res.,* **92,** 5448–5464.
——, and W. K. Dewar, 1998: Vertical mixing and cabbeling in layered models. *J. Phys. Oceanogr.,* **28,** 1458–1480.
Munk, W., 1966: Abyssal recipes. *Deep-Sea Res.,* **13,** 707–730.
Pedlosky, J., 1987: *Geophysical Fluid Dynamics.* Springer, 617 pp.
Schopf, P., and A. Loughe, 1995: A reduced-gravity isopycnal ocean model: Hindcasts of El Niño. *Mon. Wea. Rev.,* **123,** 2839–2863.
Veronis, G., 1975: The role of models in tracer studies. *Numerical Models of the Ocean Circulation,* National Academy of Sciences, 133–146.
Wunsch, C., 1996: *The Ocean Circulation Inverse Problem.* Cambridge University Press, 442 pp.